CONTRAST MEDIA & MOLECULAR IMAGING

Received: 28 January 2016, Revised: 18 August 2016, Accepted: 7 October 2016, Published online in Wiley Online Library: 15 December 2016

(wileyonlinelibrary.com) DOI: 10.1002/cmmi.1716

USPIO enhanced lymph node MRI using 3D multi-echo GRE in a rabbit model

Sung Hun Kim[a], Soon Nam Oh[a], Hyun Seok Choi[a], Hyun Sil Lee[a], Jaeseop Jun[a], Yoonho Nam[a], Sung Hak Lee[b], Jin-Kwon Lee[c] and Hae Giu Lee[a]*

Ultrasmallsuperparamagnetic iron oxide (USPIO) has been suggested to be a negative MR contrast agent to detect metastatic lymph nodes. Previously reported studies have evaluated the diagnostic performance of USPIO-enhanced MR lymph node imaging based on signal intensity. In this study, we investigate the specific performance of three different parametric approaches (normalized signal intensity, R_2* and susceptibility) using 3D multi-echo gradient echo to quantify the USPIO particles in lymph nodes. Nine rabbits with VX2 tumor implants were scanned before and after USPIO injection. From 3D multi-echo GRE magnitude and phase data, we generated multi-echo combined T_2*-weighted images, an R_2* map, and a quantitative susceptibility map. Eighteen lymph nodes (nine reactive and nine metastatic) were evaluated and showed remarkable signal drops in the area of USPIO accumulation. On parametric analysis, the R_2* difference before and after USPIO injection was significantly different ($p < 0.05$) between reactive and metastatic lymph nodes; in contrast, the normalized signal intensity and susceptibility were not significantly different between the nodes. Our study showed the potential utility of USPIO-enhanced MRI using R2* mapping from 3D multi-echo GRE for the detection of lymph node metastasis and parametric analysis of lymph node status in a rabbit model. Copyright © 2016 John Wiley & Sons, Ltd.

Keywords: lymph nodes; lymphatic metastasis; magnetite nanoparticles; rabbits; ferumoxtran-10

1. INTRODUCTION

The presence of metastatic lymph nodes is the most important prognostic factor and determines the need for radiation therapy or adjuvant chemotherapy after surgery (1). MRI and PET CT increase the diagnostic performance to identify lymph node metastases; however, one limitation is the possibility of misinterpreting enlarged reactive lymph nodes as metastases or normal sized metastatic lymph nodes as simply reactive (1–7).

Ultrasmallsuperparamagnetic iron oxide (USPIO) has been developed as a contrast agent that can be used for lymph node staging following intravenous or local subcutaneous injection (8–10). Due to the circulation of dextran-coated USPIO, it can extravasate and be absorbed physiologically in lymph nodes by macrophages, resulting in a signal loss of lymph nodes in T_2 or T_2*-weighted images. In contrast, metastatic lymph nodes exhibit this signal loss only partially or not at all depending on the extent of lymph node invasion (4,11).

In spite of its potential utility, USPIO has not yet been approved for clinical application because a prior study did not show improved specificity for detecting metastatic lymph nodes (11). Several studies have evaluated the diagnostic performance of USPIO-enhanced MRI in animal models by analyzing lymph node size and the pattern of signal intensity changes (2,4,12–15). However, the signal intensity is of relative value and signal intensity-based quantification is sensitive to several factors such as receiver coil sensitivity, susceptibility artifacts and B_1 field inhomogeneity (16). To overcome these limitations, the signal intensities were normalized by referencing the adjacent muscle signal intensities assuming USPIO accumulation is negligible in muscle tissues (15–17). Although this normalization process can reduce potential errors to some extent, a more stable and accurate parametric approach is needed.

T_2* relaxation time is another approach for quantifying USPIO accumulation because there is a linear relationship between R_2* (=1/T_2*) and iron concentration (18). Recently, quantitative susceptibility mapping (QSM) techniques, which estimate local susceptibility distributions using phase date of gradient echo (GRE) (19–21), have been suggested for *in vivo* quantification of paramagnetic contrast agent concentration (22,23). These parametric approaches using R_2* mapping or QSM may increase

* *Correspondence to: Hae Giu Lee, MD, PhD. Department of Radiology, Seoul St. Mary's Hospital, College of Medicine, The Catholic University of Korea, 222 Banpo-daero, Seocho-gu, Seoul 137-701, Korea. E-mail: hgleehfh@catholic.ac.kr*

a *S. H. Kim, S. N. Oh, H. S. Choi, H. S. Lee, J. Jun, Y. Nam, H. G. Lee*
Department of Radiology, Seoul St. Mary's Hospital, College of Medicine, The Catholic University of Korea, Seoul, South Korea

b *S. H. Lee*
Department of Hospital Pathology, Seoul St. Mary's Hospital, College of Medicine, The Catholic University of Korea, Seoul, South Korea

c *J.-K. Lee*
Department of surgery, Gyeongsang National University School of Medicine and Changwon Gyeongsang National University of Hospital, Changwon, South Korea

Abbreviations used: *USPIO, Ultrasmallsuperparamagnetic iron oxide; 2D/3D, two/three dimensional; mGRE, multi-echo Gradient Echo; QSM, quantitative susceptibility mapping; TSE, turbo spin echo; ROI, regions of interest; CFA, complete Freund's adjuvant.*

the specificity for reactive and metastatic lymph nodes. Furthermore, parametric approaches will potentially enable longitudinal studies and *in vivo* USPIO quantification.

In this study, we evaluate three different parametric approaches generated from 3D multi-echo GRE (mGRE) for USPIO-enhanced MR lymph node imaging. Using 3D mGRE magnitude and phase data, we generated multi-echo combined T_2*-weighted images, an R_2* map, and a QSM and analyzed the parameters calculated from these images for the detection of lymph node metastasis in a rabbit model.

2. MATERIALS AND METHODS

2.1. Animal preparation

This animal study was approved by the Institutional Animal Care and Use Committee. of The Catholic University of Korea College of Medicine. Nine male New Zealand white rabbits weighing 2.6–3.3 kg served as animal models. To set up a metastatic lymph node model in rabbits, we implanted four to five VX2 tumor tissue blocks (no bigger than 1 mm^3) intramuscularly in the right thigh after skin incision. For a reactive lymph node model, 0.1 mL of commercially available complete Freund's adjuvant (0.1 mg/mL, Sigma-Aldrich, Steinheim, Germany) was inoculated subcutaneously in the right medial thigh to generate lymphadenitis in the inguinal area and iliac chains.

2.2. MR contrast material

P904 (Guerbet Laboratories, Aulnay-sous-boy, France) was used in this study as the USPIO contrast agent. P904 has a smaller hydrodynamic diameter (21 nm) and a higher in vitro macrophage uptake (1.8–23 pg Fe/cell) than ferumoxtran-10 (13). P904 was used at a dose of 200 μmoL Fe/kg body weight (13). P904 has a relaxivityvalues of r1 and r2 measured in water at 1.42 T and 37 °C as 14 and 87 mM^{-1} s^{-1}, respectively (24).

2.3. MR imaging

MRI of the bilateral inguinal areas, iliac fossa and paraaortic region was performed 4 or 6 weeks after tumor implantation and 3 weeks after CFA innoculation. MRI was performed on a 3 Tesla clinical scanner (Verio, Siemens Healthcare, Erlangen, Germany) with an eight-channel knee coil. Rabbits were under full anesthesia with an intramuscular injection of 0.7 mL of ketamine hydrochloride and 0.3 mL of xylazine hydrochloride per kilogram of body weight. For contrast injection, a marginal vein in the ear was punctured by a 24-G intravenous angiocatheter system.

For all rabbits, 2D TSE and 3D mGRE images were obtained with identical imaging orientation and position. To minimize the signal contribution of fat to both magnitude and phase data, all TEs for GRE imaging were set to be multiples of the in-phase of water and fat (approximately, 2.46 ms at 3 T). Scans were performed before and after 24 hours of USPIO injection with the same protocols (12,13). A few USPIOs did not differ in the diagnostic value to discriminate the benign and malignant node at earlier acquisition time such as 120 minutes after the injection, however most USPIOs showed best and stable diagnostic value after 24 hours after injection (13). The detailed parameters for the two sequences are summarized in Table 1.

For 3D mGRE data, combined magnitude, R_2* map, and QSM were generated from multi-echo magnitude and phase data. Combined magnitude images were generated using the root sum of squares and R_2* maps were calculated using voxel-by-voxel mono-exponential fitting from multi-echo magnitude data. QSMs were reconstructed using the improved sparse linear equation and least-squares (iLSQR) technique (25) from multi-echo magnitude and phase data (STI Suite, http://people.duke.edu/~cl160).

Table 1. Pulse sequence parameters

Sequence	2D TSE (T_2)	3D mGRE (T_2*)
FOV (mm)	128	
Matrix size	256 × 256 × 40	
Voxel size (mm^3)	0.5 × 0.5 × 2.0	
Acceleration (GRAPPA)	R = 2, ACS lines =24	
TR (ms)	4000	64
TE (ms)	90	4.92, 7.38, … , 31.98
Flip angle	90 °	15 °
BW/px	219 Hz/px	501 Hz/px
ETL / # of echoes	18	12
NEX	4	2
Acqusitiontime	5:12	11:25

FOV: field of view
R: reduction factor
ACS: auto-calibraion signal
ETL: echo train length
NEX: number of excitations

2.4. Histopathological examination

After MRI, the rabbits were sacrificed for imaging-histopathologic correlation. All lymph nodes at the iliac bifurcation and the inguinal fossa were removed by one surgeon (LJK) and labeled for orientation and location then fixed in formalin (10%). A pathologist (LSH) performed hematoxylin and eosin and Prussian blue staining to visualize iron.

2.5. Image analysis

Parametric analysis was performed to compare the diagnostic performance for three different contrast images (signal intensity of the combined magnitude, R_2*, and susceptibility) generated from 3D mGRE. For confirmed lymph nodes, regions of interest (ROI) were manually drawn on representative slices of the combined magnitude images (red dotted ellipse in Fig. 1). Mean values were calculated from the defined ROIs for signal intensity, R_2*, and susceptibility. Lymph nodes very close to the bowels with a large susceptibility artifact were excluded from parametric analysis (yellow dotted arrows in Fig. 1). Table 2 summarizes the size and number of reactive and metastatic lymph nodes used in parametric analysis. For signal intensity analysis, ROIs for muscle tissues (red circles in Fig. 1) were also drawn and then the mean signal intensities of lymph node ROIs were normalized by dividing the mean signal intensities of muscle ROIs to reduce systematic errors (15).

In addition, the ratios of before and after USPIO injection were calculated for the normalized signal intensities ($SI_{ROI,after}$/$SI_{ROI,before}$, where $SI_{ROI,after}$ and $SI_{ROI,before}$ represent normalized signal intensities of lymph node ROIs after and before USPIO injection, respectively) and the differences between before and after USPIO injection were calculated for R_2*

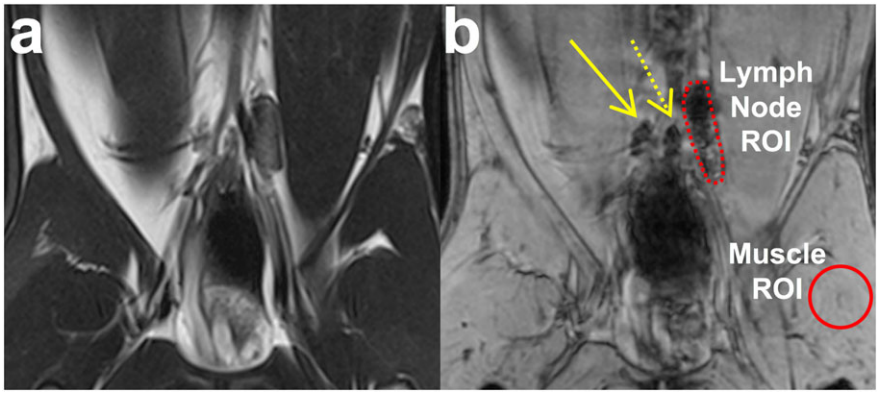

Figure 1. (**a**) T_2-weighted magnitude image of 2D TSE and (**b**) T_2*-weighted multi-echo combined magnitude image of 3D mGRE 24 hours after USPIO injection. Three reactive lymph nodes (yellow arrows and red dotted ellipse) were confirmed by histopathology after MR examination. The combined magnitude image of 3D mGRE shows the entire signal loss in all three reactive nodes.

Table 2. Size of lymph nodes used in parametric analysis

	Long-axis (mm)		Short-axis (mm)	
	Mean (S.D.)	Range	Mean (S.D.)	Range
Reactive (n = 9)	8.8 (3.5)	5.0 – 16.0	4.4 (2.2)	2.0 – 9.0
Metastatic (n = 9)	12.5 (5.3)	5.0 – 20.0	7.5 (1.9)	4.7 – 10.5

S.D. standard deviation.

(R_2*$_{ROI,after}$ - R_2*$_{ROI,before}$, where R_2*$_{ROI,after}$ and R_2*$_{ROI,before}$ representR_2*s of lymph node ROIs after and before USPIO injection, respectively) and susceptibility ($QSM_{ROI,after}$ - $QSM_{ROI,before}$, where and represent QSMs of lymph node ROIs after and before USPIO injection, respectively). For the calculated mean values of the normalized signal intensities, R_2*, and susceptibility, a Mann-Whitney U test was performed between reactive and metastatic lymph nodes. All post-processing steps were performed using MATLAB (MathWorks Inc., Natick, MA, USA).

3. RESULTS

Twenty-nine lymph nodes (18 reactive and 11 metastatic) were isolated from nine rabbits after MR examination. Among them, 11 lymph nodes near the bowel (nine reactive and two metastatic) were excluded from parametric analysis due to severe susceptibility artifacts from bowel gas. The sizes of reactive and metastatic lymph nodes analyzed in this study are summarized in Table 2.

Fig. 2 shows representative slices including a metastatic lymph node for T_2-weighted magnitude (2D TSE) and different contrast images generated using 3D mGRE data (combined magnitude, R_2* map, phase, QSM) before and after USPIO injection. Although remarkable signal changes were observed in the combined magnitude, R_2* map, phase, and QSM at the boundaries of the lymph nodes (arrowheads in Fig. 2) 24 hours after USPIO injection, signal changes were relatively small in the inside regions of the metastatic lymph nodes (red arrows in Fig. 2).

Fig. 3 shows the different patterns of the phase and QSM images for reactive and metastatic lymph nodes. After USPIO injection, both lymph nodes showed partial signal losses mainly at boundary regions in the magnitude images. The phase and

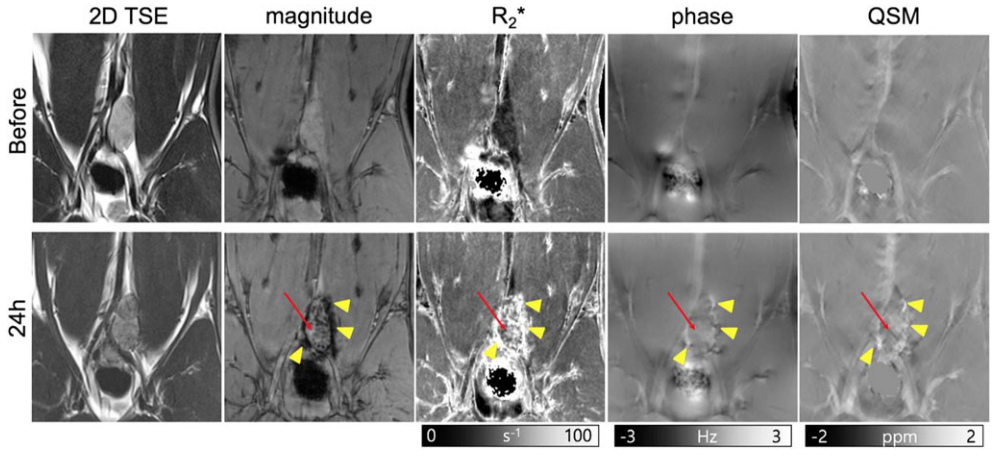

Figure 2. Comparison of different contrast images before and after USPIO injection. Noticeable signal changes in the boundary voxels of a metastatic lymph node (yellow arrow heads) are shown in the combined magnitude, R_2* map, phase and QSM 24 hours after USPIO injection.

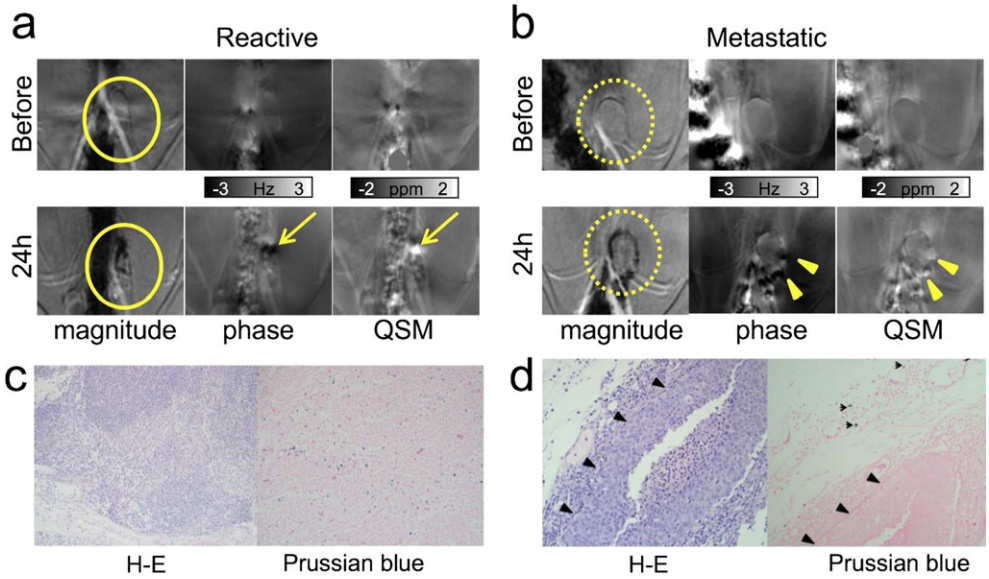

Figure 3. Signal patterns of phase and QSM for (**a**) reactive and (**b**) metastatic lymph nodes. The corresponding hematoxylin-eosin (H-E) and Prussian blue staining photomicrographs (×400) are displayed for (**c**) reactive and (**d**) metastatic lymph nodes. Histopathology demonstrates the metastatic lymph node (arrowheads in Fig. 3d) devoid of iron content and a small fleck of iron (arrows in Fig. 3d) at the surrounding stroma.

QSM depict more localized patterns for metastatic lymph nodes (arrowheads in Fig. 3b). In QSM, blooming effects shown in the magnitude and phase images are markedly reduced and positive signs (arrow and arrowheads in Fig. 3a and 3b) suggest the presence of paramagnetic susceptibility sources with more accurate localization for both nodes after USPIO injection. The histopathologiesdemonetrate diffuse iron contents for the corresponding reactive lymph node (blue spots in Fig. 3c). Whereas the metastatic tumor cells are devoid of iron content and a small fleck of iron is seen at the surrounding stroma (blue spots in Fig. 3d).

In parametric analysis, all three different contrasts showed noticeable changes 24 hours after USPIO injection for both reactive and metastatic lymph nodes, as shown in Fig. 4. The R_2* difference before and after USPIO injection was significantly different ($p < 0.05$) between reactive and metastatic lymph nodes. While normalized signal intensity and susceptibility did not show significant differences between reactive and metastatic lymph nodes, they did show visually different signal patterns for most lymph nodes after USPIO injection. The mean and standard deviation calculated from the ROIs for three different contrasts are summarized in Table 3.

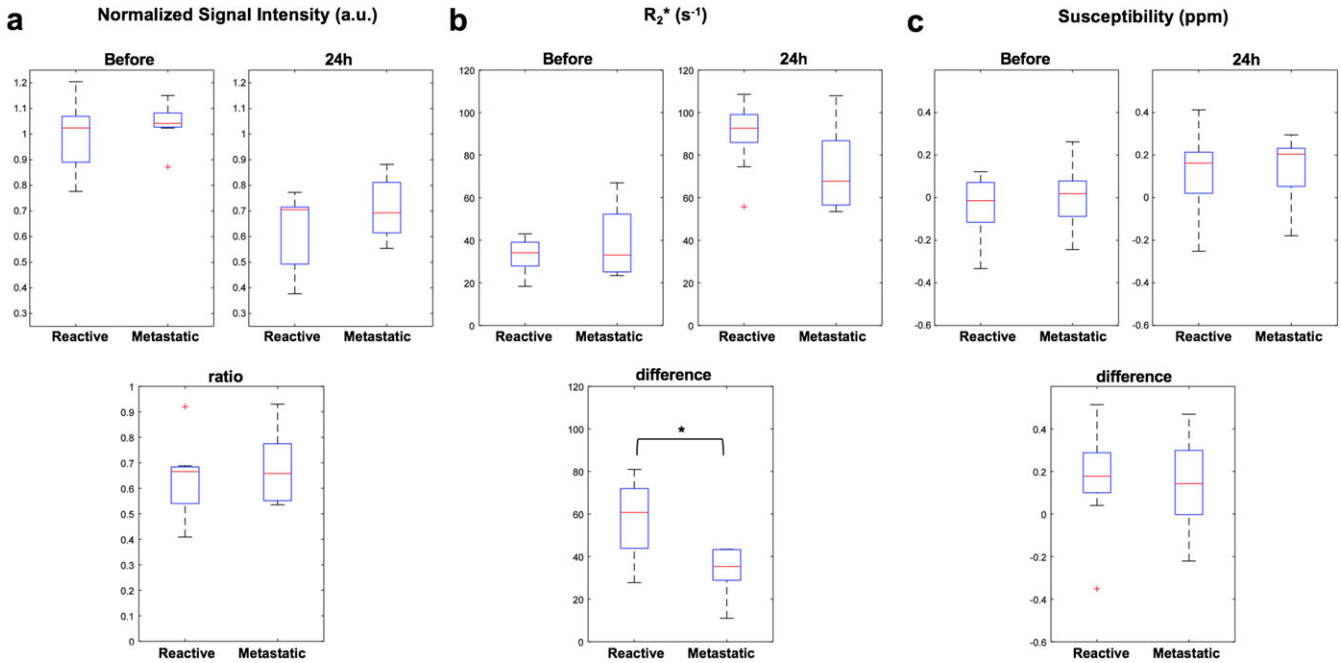

Figure 4. ROI-based quantification results of reactive and metastatic lymph nodes for (**a**) normalized signal intensity of magnitude image, (**b**) R_2*, and (**c**) susceptibility (* $p < 0.05$).

Table 3. Parametric analysis: ROI mean values (standard deviation) of normalized signal intensity, R_2* and susceptibility (χ) before and 24 hours after USPIO injection

	Normalized S.I. (a.u.)			R_2* (s^{-1})			χ (ppm)		
	before	24 h	ratio	before	24 h	ΔR_2*	before	24 h	$\Delta\chi$
Reactive	0.99	0.62	0.63	33.0	89.5	56.5	-.04	.13	0.17
(n = 9)	(0.14)	(0.14)	(0.14)	(7.7)	(15.7)	(18.4)	(0.15)	(.19)	(0.25)
Metastatic	1.04	0.71	0.69	39.8	73.8	34.0	.01	.14	0.13
(n = 9)	(0.08)	(0.12)	(0.14)	(17.4)	(19.1)	(10.8)	(.15)	(.15)	(0.23)
***p*-value**	0.3865	0.3401	.6048	0.7962	0.0939	.0106	0.6665	0.6488	.7304

ratio: the normalized signal intensity ratios of before and after USPIO injection ($SI_{ROI,after}/SI_{ROI,before}$)
ΔR_2*: the R_2* differences between before and after USPIO injection ($R_2*_{ROI,after} - R_2*_{ROI,before}$)
$\Delta\chi$: the QSM differences between before and after USPIO injection ($QSM_{ROI,after} - QSM_{ROI,before}$)
p-values were calculated by using a Mann-Whitney U test.

4. DISCUSSION

We investigated the ability to discriminate lymph nodes with three different parametric approaches of normalized signal intensity (T_2*-weighted multi-echo combined magnitude), R_2* map, and QSM. For this purpose, 3D mGRE images were acquired before and after USPIO injection in a rabbit model. Among them, only the difference in R_2* values before and after USPIO injection showed a significant difference between reactive and metastatic lymph nodes.

The combined magnitude, R_2* map, phase and QSM generated using 3D mGRE data showed remarkable signal changes in the USPIO accumulation area after USPIO injection. In the case of metastatic lymph nodes, remarkable signal changes were observed at the lymph node boundaries; however, signal changes were relatively small in the inside regions. These results are in accordance with those of previous lymph node studies using USPIO (7,15). In the present study, we observed different patterns for reactive and metastatic lymph nodes in the phase and QSM images. After USPIO injection, both lymph nodes showed partial signal loss mainly at the boundary regions in the magnitude images. However, there were more localized patterns minimizing nonlocal signal changes due to susceptibility artifacts for metastatic lymph nodes in comparison with reactive lymph nodes. These results suggest that relatively sparse USPIO distribution in the metastatic lymp nodes. In addition, QSM showed markedly decreased blooming effects as compared with the magnitude and phase images and high signal positive signs, suggesting the presence of paramagnetic susceptibility sources.

R_2* measurement can be used to quantify USPIO nanoparticles at a relatively low iron concentration (12). However, in the presence of a high iron concentration, relaxometry-based approaches are almost impossible when using regular pulse sequences and aggregations of SPIO nanoparticles could drastically influence local relaxation time, making quantification more complicated (26). Further studies to optimize imaging parameters (e.g., shortest echo time) and USPIO concentration will be required to quantify a wide range of lymph nodes.

In the present study, the normalized signal intensity did not show significant differences between reactive and metastatic lymph nodes. Our results did not correspond to previous results that benign nodes had a significantly lower signal intensity ratio than metastatic nodes (2,12). This discordance among studies might be derived from the sample size, MR machine and sequence, the presence of the intervention to minimize the susceptibility artifact and different contrast agents.

We expected that reactive lymph nodes would show a higher QSM value; however, our results did not demonstrate significant differences. These results were probably due to an inherent limitation of this sequence. MR phase can be affected by many other sources, including fat signal contribution (27,28), physiological motion such as cardiac motion, blood flow during phase encoding (29), large scale susceptibility artifacts due to a wide range of USPIO concentration (30) and initial phase induced by RF excitation (31). These unwanted phase sources can highly affect the quality of the background phase removal and QSM processes which solve ill-posed inverse problem (18–20). The effects of these should be investigated and controlled for lymph node quantification using QSM. In this study, the reactive lymph nodes were more affected by these effects (mainly from bowel gas and respiration) compared to the metastatic lymph nodes, thus 50% of the reactive lymph nodes were excluded in parametric analysis due to severe artifacts in magnitude and phase images. Although the other 50% of the reactive lymph nodes were included in parametric analysis, many of them show noisy QSM results compared to those of the metastatic lymph nodes.

One limitation of this study is the relatively small number of lymph nodes sampled, particularly in quantification evaluation. The resulting contrast images visualized the lymph nodes and demonstrated the signal changes in the areas of USPIO accumulation. However, among 29 lymph nodes, 11 lymph nodes near the bowel (37.9%) were excluded from parametric analysis due to severe susceptibility artifacts from bowel gas. Thus, the final number of samples may be insufficient for revealing subtle differences in the various quantification values.

In conclusion, USPIO-enhanced MRI using R2* mapping from 3D multi-echo GRE has the potential utility for the detection of lymph node metastasis and parametric analysis of lymph node status in a rabbit model.

Acknowledgements

This research was supported by the Radiology Research Foundation Program of College of Medicine at the Catholic University of Korea 2014.

REFERENCES

1. Weissleder R, Elizondo G, Wittenberg J, Lee AS, Josephson L, Brady TJ. Ultrasmall superparamagnetic iron oxide: an intravenous contrast agent for assessing lymph nodes with MR imaging. Radiology 1990; 175: 494–498.
2. Bellin MF, Roy C, Kinkel K, Thoumas D, Zaim S, Vanel D, Tuchmann C, Richard F, Jacqmin D, Delcourt A, Challier E, Lebret T, Cluzel P. Lymph node metastases: safety and effectiveness of MR imaging with ultrasmall superparamagnetic iron oxide particles – initial clinical experience. Radiology 1998; 207: 799–808.
3. Anzai Y, Blackwell KE, Hirschowitz SL, Rogers JW, Sato Y, Yuh WT, Runge VM, Morris MR, McLachlan SJ, Lufkin RB. Initial clinical experience with dextran-coated superparamagnetic iron oxide for detection of lymph node metastases in patients with head and neck cancer. Radiology 1994; 192: 709–715.
4. Kinner S, Maderwald S, Albert J, Parohl N, Corot C, Robert P, Baba HA, Barkhausen J. Discrimination of benign and malignant lymph nodes at 7.0 T compared to 1.5 T magnetic resonance imaging using ultrasmall particles of iron oxide: a feasibility preclinical study. Acad Radiol 2013; 20: 1604–1609.
5. Lee JY, Choi BI, Son KR, Lee JM, Kim SJ, Park HS, Chang JM, Choi SH, Kim MA, Moon WK. Lymph node metastases from gastric cancer: gadofluorine M and gadopentetate dimeglumine MR imaging in a rabbit model. Radiology 2012; 263: 391–400.
6. Antoch G, Stattaus J, Nemat AT, Marnitz S, Beyer T, Kuehl H, Bockisch A, Debatin JF, Freudenberg LS. Non-small cell lung cancer: dual-modality PET/CT in preoperative staging. Radiology 2003; 229: 526–533.
7. Choi SH, Moon WK, Hong JH, Son KR, Cho N, Kwon BJ, Lee JJ, Chung JK, Min HS, Park SH. Lymph node metastasis: ultrasmall superparamagnetic iron oxide-enhanced MR imaging versus PET/CT in a rabbit model. Radiology 2007; 242: 137–143.
8. Ittrich H, Peldschus K, Raabe N, Kaul M, Adam G. Superparamagnetic iron oxide nanoparticles in biomedicine: applications and developments in diagnostics and therapy. Rofo 2013; 185: 1149–1166.
9. Alecci M, Collins CM, Smith MB, Jezzard P. Radio frequency magnetic field mapping of a 3 Tesla birdcage coil: experimental and theoretical dependence on sample properties. Magn Reson Med 2001; 46: 379–385.
10. Choi SH, Kim KH, Moon WK, Kim HC, Cha JH, Paik JH, Chang KH. Comparison of lymph node metastases assessment with the use of USPIO-enhanced MR imaging at 1.5 T versus 3.0 T in a rabbit model. J Magn Reson Imaging 2010; 31: 134–141.
11. Weissleder R, Stark DD, Engelstad BL, Bacon BR, Compton CC, White DL, Jacobs P, Lewis J. Superparamagnetic iron oxide: pharmacokinetics and toxicity. AJR Am J Roentgenol 1989; 152: 167–173.
12. Ziener CH, Bauer WR, Jakob PM. Transverse relaxation of cells labeled with magnetic nanoparticles. Magn Reson Med 2005; 54: 702–706.
13. Marques J, Bowtell R. Application of a Fourier-based method for rapid calculation of field inhomogeneity due to spatial variation of magnetic susceptibility. Concepts Magn Resonance Part B: Magn Reson Eng 2005; 25: 65–78.
14. de Rochefort L, Brown R, Prince MR, Wang Y. Quantitative MR susceptibility mapping using piece-wise constant regularized inversion of the magnetic field. Magn Reson Med 2008; 60: 1003–1009.
15. Shmueli K, de Zwart JA, van Gelderen P, Li TQ, Dodd SJ, Duyn JH. Magnetic susceptibility mapping of brain tissue in vivo using MRI phase data. Magn Reson Med 2009; 62: 1510–1522.
16. Xu B, Spincemaille P, Liu T, Prince MR, Dutruel S, Gupta A, Thimmappa ND, Wang Y. Quantification of cerebral perfusion using dynamic quantitative susceptibility mapping. Magn Reson Med 2015; 73: 1540–1548.
17. Bonekamp D, Barker PB, Leigh R, van Zijl PC, Li X. Susceptibility-based analysis of dynamic gadolinium bolus perfusion MRI. Magn Reson Med 2015; 73: 544–554.
18. Kinner S, Maderwald S, Albert J, Parohl N, Corot C, Robert P, Baba HA, Barkhausen J. Comparison of two different iron oxide-based contrast agents for discrimination of benign and malignant lymph nodes. Invest Radiol 2012; 47: 511–515.
19. Sigovan M, Boussel L, Sulaiman A, Sappey-Marinier D, Alsaid H, Desbleds-Mansard C, Ibarrola D, Gamondes D, Corot C, Lancelot E, Raynaud JS, Vives V, Lacledere C, Violas X, Douek PC, Canet-Soulas E. Rapid-clearance iron nanoparticles for inflammation imaging of atherosclerotic plaque: initial experience in animal model. Radiology 2009; 252: 401–409.
20. Yoo RE, Cho HR, Choi SH, Won JK, Kim JH, Sohn CH. Optimization of Ultrasmall Superparamagnetic Iron Oxide (P904)-enhanced Magnetic Resonance Imaging of Lymph Nodes: Initial Experience in a Mouse Model. Anticancer Res 2014; 34: 5389–5396.
21. Li W, Wang N, Yu F, Han H, Cao W, Romero R, Tantiwongkosi B, Duong TQ, Liu C. A method for estimating and removing streaking artifacts in quantitative susceptibility mapping. Neuroimage 2015; 108: 111–122.
22. Wang L, Potter WM, Zhao Q. In vivo quantification of SPIO nanoparticles for cell labeling based on MR phase gradient images. Contrast Media Mol Imaging 2015; 10: 43–50.
23. Yoo RE, Choi SH, Cho HR, Jeon BS, Kwon E, Kim EG, Park J, Myeong WJ, Won JK, Lee YS, Kim JH, Park SW, Sohn CH. Magnetic resonance imaging diagnosis of metastatic lymph nodes in a rabbit model: efficacy of PJY10, a new ultrasmall superparamagnetic iron oxide agent, with monodisperse iron oxide core and multiple-interaction ligands. PLoS One 2014; 9 e107583.
24. Sharma SD, Hernando D, Horng DE, Reeder SB. Quantitative susceptibility mapping in the abdomen as an imaging biomarker of hepatic iron overload. Magn Reson Med 2015; 74(3): 673–683.
25. Dimov AV, Liu T, Spincemaille P, Ecanow JS, Tan H, Edelman RR, Wang Y. Joint estimation of chemical shift and quantitative susceptibility mapping (chemical QSM). Magn Reson Med 2015; 73(6): 2100–2110.
26. Nam Y, Kim DH, Lee J. Physiological noise compensation in gradient-echo myelin water imaging. Neuroimage 2015; 120: 345–349.
27. Wang L, Potter WM, Zhao Q. In vivo quantification of SPIO nanoparticles for cell labeling based on MR phase gradient images. Contrast Media Mol Imaging 2015; 10(1): 43–50.
28. Kim DH, Choi N, Gho SM, Shin J, Liu C. Simultaneous imaging of *in vivo* conductivity and susceptibility. Magn Reson Med 2014; 71(3): 1144–1150.
29. Islam T, Harisinghani MG. Overview of nanoparticle use in cancer imaging. Cancer Biomark 2009; 5: 61–67.
30. Shen N, Tan J, Wang P, Wang J, Shi Y, Lv W, Xie X, Huang X. Indirect magnetic resonance imaging lymphography identifies lymph node metastasis in rabbit pyriform sinus VX2 carcinoma using ultra-small super-paramagnetic iron oxide. PLoS One 2014; 9 e94876.
31. Lei J, Xue HD, Li Z, Li S, Jin ZY. Possible pathological basis for false diagnoses of lymph nodes by USPIO-enhanced MRI in rabbits. J Magn Reson Imaging 2010; 31: 1428–1434.